

# The Modelling of Mechanical Heart Valve Closure Dynamics

In-vitro Evaluation of a Doppler Ultrasound Technique  
for the Measurement of Closure Velocities of a  
Björk-Shiley MHV

David Henry Pinney BSc

A thesis submitted to the University of Sheffield  
in partial fulfillment of the requirements for the degree of  
MSc Medical Physics and Clinical Engineering



Undertaken mainly in the Department of Medical Physics and  
Clinical Engineering, University of Sheffield.

July 2004

# Abstract

This three student project set out to investigate tools for the modelling of the closure event of Mechanical Heart Valves.

This part of the study aimed to investigate the possibility of determining the closing speeds of a Mechanical Heart Valve (MHV) in an *in-vitro* environment, using Continuous Wave (CW) Doppler Ultrasound. The closing speed of the MHV leaflets provides important information for the calculation of the dynamic stresses and potential structural damage to the valve.

The first main part of the project aims to use Continuous Wave Doppler ultrasound to measure the velocities involved over the course of the valve closure event. It is anticipated that the closure event has a duration of the order of a few milliseconds. This part of the project is to be further sub-divided into two distinct parts to be carried out by different members of the project team: one to construct and evaluate a suitable test-rig to hold an artificial heart valve rigidly such that a study of the heart-valve dynamics can be undertaken by coupling it with the ultrasound probe. The other sub-part is to devise a method of extracting the information from the analogue output of the ultrasound machine suitable for producing a velocity/time profile in a Personal Computer (PC).

A Shelhigh accelerated rate fatigue tester was used during the course of this study, along with a Huntleigh Healthcare Multi-Dopplex 2 hand-held Doppler ultrasound machine. These were used to investigate the motion of a simple spring-loaded valve and a Björk-Shiley (BS) monostrut valve. It was found that under the conditions used, the BS valve had a peak closing velocity of between approximately 10cm/s and 17cm/s depending on the simulated heart rate.

The second main part of the project, carried out by the third member of the project team, aims to combine solid and fluid mechanics of the complex heart valve motion and solve them together in a single computational package, Field Operations And Manipulations (FOAM). This could lead eventually to modelling of the heart valve closure dynamics computationally. This can be sub-divided into solving the Poiseuille's equations, leading to modelling of pulsatile flow in an elastic tube and then applying this to artificial heart-valve closure.

# Acknowledgements

I would like to acknowledge the help and support of several people:

- Dr R. Hose and Dr P. Lawford as primary supervisors for their guidance throughout the project.
- Dr. R. Walker of the Medical Physics section at the Northern General Hospital for his invaluable help and advice in all things ultrasound and the use of a lab at the Northern General Hospital (NGH) for the ultrasound calibration.
- Dr. J. Fenner for his help when we inevitably got stuck with signal processing.
- The staff of the Biomedical Workshop, Royal Hallamshire Hospital (RHH) for their ability to understand my hand-waving and produce work of a great standard, often in tight time-scales.
- Devi Ravindranathan my project partner for this part of the project, for not always letting me win our arguments.
- And finally Charlotte, my wife, for her constant support through this hectic and sometimes difficult time.

# Personal Statement

## Project Description

The heart valve closure is a complex event. By gaining details of the mechanisms, velocities and forces involved, a greater understanding of the reasons for heart valve failures can be achieved.

## Project Aims

The aims of my part of the project are to:

- Investigate Order of Magnitude figures for velocities involved in the heart-valve closure event.
- Investigate the suitability of a heart valve wear tester for this project
- Design suitable modifications for heart valve wear tester to accommodate a Doppler ultrasound probe
- Test and evaluate modifications
- Study closure event of translate only (spring-loaded) heart-valve mounted in the wear-tester
- Study closure event of Björk-Shiley heart-valve mounted in the wear-tester
- Draw suitable conclusions and recommendations for further work

# Contents

<b>Abstract</b>	<b>i</b>
<b>Acknowledgements</b>	<b>ii</b>
<b>Personal Statement</b>	<b>iii</b>
<b>1 Introduction and Literature Review</b>	<b>1</b>
1.1 History and Evolution of Mechanical Heart Valves . . . . .	1
1.1.1 Ball Valves . . . . .	2
1.1.2 Single Disc Valves . . . . .	3
1.1.3 Bi-leaflet Valves . . . . .	4
1.2 Heart Valve Failure . . . . .	5
1.2.1 Aortic and Mitral Valve Failure . . . . .	5
1.2.2 MHV Failure . . . . .	5
1.3 Current Position on Heart Valve Closure Measurement . . . . .	6
1.4 Computer Modelling of the FSI of Heart Valve Dynamics . . . . .	7
1.5 Background to this Project . . . . .	7
<b>2 Technology Used and its Limitations</b>	<b>9</b>
2.1 Doppler Ultrasound . . . . .	9
2.1.1 The Doppler Effect . . . . .	9
2.1.2 Doppler Systems: Overview . . . . .	10
2.1.3 Continuous Wave Doppler Systems . . . . .	11
2.1.4 Ultrasound Transducers, Fields and Beams . . . . .	11
2.2 Huntleigh MD2 Hand-held Doppler Ultrasound Machine . . . . .	12
2.3 Membrane Hydrophone . . . . .	13
2.4 Laptop Computer and Sound Card Input . . . . .	13
2.5 String Phantom for Doppler Quality Assurance . . . . .	14
<b>3 Characterisation of Doppler Machine</b>	<b>15</b>
3.1 Ultrasound Beam Characterisation . . . . .	15
3.1.1 Experimental Setup . . . . .	15
3.1.2 Experimental Procedure . . . . .	15
3.1.3 Results . . . . .	17
3.2 Determination of the Audio Card Response . . . . .	19
3.2.1 Experimental Methods . . . . .	19
3.2.2 Signal Processing Methods . . . . .	21
3.2.3 Results . . . . .	22

3.3	Determination of the Doppler Response . . . . .	23
3.3.1	Experimental Methods . . . . .	23
3.3.2	Statistical Methods . . . . .	23
3.3.3	Results . . . . .	26
<b>4</b>	<b>Using a Wear Tester to Study Closure</b>	<b>28</b>
4.1	The Shelhigh Accelerated Rate Wear Tester . . . . .	28
4.1.1	Description of Accelerated Wear Systems . . . . .	28
4.1.2	Modifications Required . . . . .	29
4.2	Using a Spring-Loaded Translation Valve . . . . .	30
4.2.1	Experimental Methods . . . . .	30
4.2.2	Signal Processing Methods . . . . .	31
4.2.3	Results . . . . .	32
4.2.4	Verification of Results . . . . .	32
4.3	Using the Björk-Shiley Tilting-disc Valve . . . . .	34
4.3.1	Methods . . . . .	34
4.3.2	Results . . . . .	34
4.3.3	Verification of Results . . . . .	38
<b>5</b>	<b>Conclusions and Discussion</b>	<b>40</b>
5.1	US Beam from Dopplex Machine . . . . .	40
5.2	Laptop Computer Audio Response . . . . .	40
5.3	Doppler Signal and Interface with PC . . . . .	40
5.4	Using US Machine to Detect Heart Valve Motion . . . . .	41
5.5	Use of Doppler Techniques for Detecting MHV Failure . . . . .	42
5.6	Suggestions for Further Work . . . . .	42
<b>A</b>	<b>Project Plans</b>	<b>45</b>
<b>B</b>	<b>MATLAB Programs used</b>	<b>48</b>
B.1	Frequency Analysis Program . . . . .	48
B.2	Moving Window & Speed Calculations . . . . .	49
<b>C</b>	<b>MATLAB Specgram Function</b>	<b>51</b>
C.1	Syntax . . . . .	51
C.2	Description . . . . .	51
C.3	Algorithm . . . . .	53

# Chapter 1

## Introduction and Literature Review

It is known that the heart, in every-day conversation is synonymous with love and life, but it has many other associations too. For example 'have a heart' means to be merciful, and 'have your heart in the right place' means to be kind, while 'heavy heart' refers to sadness.

No other bodily organ elicits this kind of response. When was the last time you had a heavy pancreas?

*Adapted from*

*<http://www.howstuffworks.com/heart.htm>*

### 1.1 History and Evolution of Mechanical Heart Valves

Cardiac valves have three main functions:

1. Preventing regurgitation of blood from the ventricle to the atria (mitral valve) or from the aorta back into the ventricle (aortic valve).
2. Permit high speed flow through the valve without impeding the flow.
3. Withstand high pressure loads from the attempted back-flow of blood.

The aim of using a MHV prosthesis is to replace the normal action of the natural valve with that of a replacement when the action of the natural valve becomes abnormal.

### 1.1.1 Ball Valves

The need for artificial Mechanical Heart Valves (MHVs) was long recognised, but it was not possible before 1952. After a full and proper investigation, Dr. Charles Hufnagel first used a contained ball valve in October of that year. It was placed in the descending thoracic aorta for treatment of an aortic valvular insufficiency. This valve worked by having a ball sit at the proximal end of a tube during diastole such that it forms a seal and three pouches that open around the ball in its systolic position in the distal portion of the tube[1]. This allows blood to flow in one direction only. No anticoagulation therapies were used and some Hufnagel ball valves were recovered up to 30 years after implantation with no visible wear.

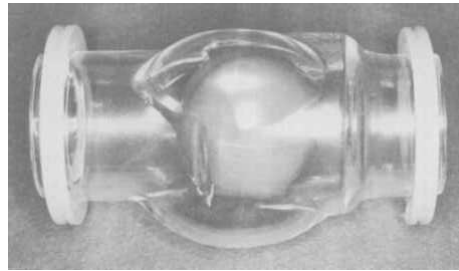


Figure 1.1: Hufnagel Contained Ball valve

In 1960, Dr. A. Starr and Lowell Edwards came together and designed a caged ball valve with a methacrylate cage and silicon rubber ball. A cast Stellite-21 cage soon replaced the methacrylate as it proved to be biocompatible. The silicon rubber balls used in the early versions absorbed lipids, ultimately leading to the ball changing its shape and subsequent valve failures; from 1965, the silicon rubber balls were made using a different curing process which relieved these problems. The Starr-Edwards caged ball valve is still in use today, essentially unchanged, particularly in the third world countries because of its reasonable cost[2]. The tilting disc and bileaflet valves that appeared in the 1970s offer superior haemodynamic performance, although the Starr-Edwards ball valve has proved to be quite satisfactory in the mitral position.

The DeBakey-Surgitool ball valve, introduced in 1967, has a similar design to the Starr-Edwards ball valve, except that the ball is a hollow Pyrolytic carbon poppet. This was the first use in heart valves of a new carbon material developed



Figure 1.2: Starr-Edwards Caged-Ball valve

at the General Atomic Company in California. The Pyrolyte ball was used in a titanium cage, but caused excessive wear to the struts leading to its eventual discontinuation.

Pyrolytic carbon, originally developed for containing nuclear fuel rods has now become the principal biomaterial for virtually all new mechanical valves. Over 2 million valves with Pyrolyte components have been used since its introduction.

### 1.1.2 Single Disc Valves

One of the first disc valves, introduced in the early 1960s, was the Kay-Shiley non-tilting disc valve. Other similar non-tilting disc valves included the Beall-Surgitool disc valve and the Cooley-Cutter biconical disc valve.



Figure 1.3: (a) Beall-Surgitool valve. (b) Cooley-Cutter biconical valve.

The first tilting disc valves were of the Lillehei-Cruz-Kaster type introduced in 1963. These had a free-floating disc, retained by a shaped cage. The Lillehei-Kaster tilting disc prosthesis was an improvement of this; the pivot point was moved and the cage was replaced with lateral guides. Subsequent improvements, with the guides being further reduced with abbreviated earlike guards, produced the Omniscience and Omnicarbon valves, both of which are still in use.

The Björk-Shiley (BS) tilting disc valve utilised two U-shaped wire struts welded to a Stellite orifice as the disc retainer, together with a Pyrolyte disc. The convexo-concave versions of these valves suffered as the outlet retainer



Figure 1.4: The Lillehei-Kaster tilting disc valve.

occasionally fractured at its weld joint, releasing the disc. This was rectified by the use of a mono-strut that was machined as an integral part of the surrounding ring, therefore involving no welded joint at this point[3].

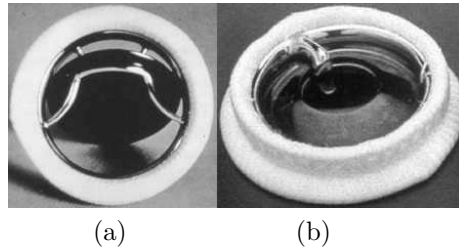


Figure 1.5: (a) Björk-Shiley Convex-Concave valve. (b) Björk-Shiley monostrut valve.

Dr. K.V. Hall of Norway was a cardiac surgeon in the mid-1970s when he believed that improvements could be made to the tilting-disc valves available at that time. He teamed up with Mr. Woien and Mr. Kaster to produce a tilting-disc valve incorporating a Pyrolyte disc with a small hole in the centre. A wire passed through this hole, such that the hole was occluded when the valve was in the closed position. This wire acted as a guide for the disc to slide along to tilt open. This valve later became the Medtronic-Hall valve.

### 1.1.3 Bi-leaflet Valves

The main drive behind the development of the bileaflet valves, was to provide a lower profile than the large caged-ball valves available in the early 1960s. Various designs for these are discussed by DeWall *et al*[1] and Gott *et al*[2]. The original design of the St Jude Medical bileaflet valve has remained almost unchanged since its introduction in 1977. This is now the most widely used



Figure 1.6: The Medtronic-Hall tilting disc valve.

prosthetic valve in the world[2].



Figure 1.7: St. Jude Medical bi-leaflet valve.

## 1.2 Heart Valve Failure

### 1.2.1 Aortic and Mitral Valve Failure

Valvular Heart Disease (VHD), a generic name given to various diseases affecting the heart valves, can be classified into congenital (present from birth) and acquired. Acquired VHD is much more common than congenital and is caused by a disease, or injury to the heart[4].

Primary valve failure can occur suddenly due to tearing or breakage of the valve leaflets, or, over a longer period of time due to calcification or thrombus formation.

There are two main reasons for a patient undergoing valvular replacement: the valve may not close fully, leaking blood under back flow (regurgitation); and the valve may become hardened so does not open properly (stenosis)

### 1.2.2 MHV Failure

Mechanical valves are exposed to a hostile environment with respect to the pressures and forces exerted on them when implanted into the body and therefore

parts of the valve can have large stresses placed upon them; this can, in some cases, lead to failure of the MHV. Causes of valve failure are highly patient specific.

To further understand these failure modes of MHVs, it is necessary to understand the speeds and forces involved during the closure event of the valve leaflets.

### 1.3 Current Position on Heart Valve Closure Measurement

There have been several studies into the closure dynamics of various MHVs. Lee *et al*[5], Wu *et al*[6], Guo *et al*[7], Chandran and Aluri[8] all used a laser sweeping technique to measure the velocity of closure of various MHV leaflets over the last few degrees before occluder impact. These studies were conducted in a state where pulse rates, flow rates and pressures were representative of a physiological environment. Most of these investigations conclude that under physiological conditions, the occluder of a single leaflet valve approaches closure at around  $1.5\text{--}2.0\text{ms}^{-1}$ .

Several papers published have also looked at occluder closure with respect to cavitation inception in the fluid around the valve[5, 6, 7, 8, 9]. This is an important consideration in the measurement of valve closure events, as cavitation can cause serious damage to MHVs and their surrounding environment. Such damage includes causing surface pitting which can lead to thrombus formation and in the worst case, causing the leaflet or valve mounting ring to crack, leading to total valve failure. Lee *et al*[5] describe the action of cavitation inception and the effect it can have on materials near to the cavitation bubbles.

It has been noted above that the Björk-Shiley Convexo Concave (BSCC) valve suffered from outlet strut fracture in a small percentage of patients. Some studies have been conducted looking at the impact forces on the outlet struts of these valves[10, 11]. Chandran *et al*[10] used BSCC 29mm valves instrumented with strain gauges on the outlet strut legs to measure the forces on the struts and a fibre optic trigger to measure the average velocity of the occluder tip over approximately the last 1cm of its closure. They found that the average tangential velocity of the occluder tip to be around  $2.3\text{ms}^{-1}$  and was not significantly affected by the fluid flow rate. Eberhardt *et al*[11] investigated the relationship

between closure delay, occluder velocity and outlet strut forces, by measuring the disc rotation near closing using a miniature non-contact photo proximity sensor. This revealed an “over-rotation” phenomenon, where at the point of closure, the occluder over-rotates slightly, oscillates briefly and settles into a closed resting position around 5ms after initial contact. They also observed that the closing does not occur at precisely the same time in each cycle, but varies over a range of approximately 20ms and that the peak over-rotation of the occluder increases with a greater delay. For these late closures, the occluder velocity is also higher. They noted that a closure delay of 20ms can result in an approximate doubling of the arresting forces applied to the outlet strut and concluded that closure delay is significant to the loading of the outlet strut.

## 1.4 Computer Modelling of the FSI of Heart Valve Dynamics

The third member of our project team, Constantinos Zervides, has attempted to computationally model the valve closure dynamics using a software package called “Field Operations And Manipulations” (FOAM), a software tool with fully coupled Fluid-Solid Interaction (FSI) solvers. Closure dynamics of a heart valve is a complex motion which includes both solid and fluid mechanics in a fully coupled solution; the pressure distributions involve fluid dynamics while the disc motion is a solid mechanics problem. Most of the existing software solutions solve the solid and fluid mechanics problems in separate packages, with results being passed between them. FOAM enables them to be solved together. He has studied the FSI in an elastic tube and solved Poiseuille’s equation using FOAM. The details of his work are however out of the scope of this project report.

## 1.5 Background to this Project

The details of the in-vitro evaluation of the closing velocities of the Björk-Shiley Convexo Concave (BSCC) heart valve using the Continuous Wave (CW) Doppler ultrasound will be dealt in detail in the following chapters of this report.

The Department of Medical Physics and Clinical Engineering at the University of Sheffield has access to a Huntleigh Healthcare hand-held Continuous Wave (CW) ultrasound machine. These are usually used in the assessment of blood flow in vessels for example in Peripheral Arterial Disease, the Diabetic

foot, and other venous problems. One of the project aims is to assess whether CW ultrasound can be used to detect the motion of the MHV leaflet in a laboratory *in-vitro* environment. If this proves successful, it is ultimately hoped that transoesophageal ultrasound can be used to assess the motion of MHV leaflets.

The project plans for this project are shown in appendix A, along with an explanation of the changes made during the course of the project.

## Chapter 2

# Technology Used and its Limitations

### 2.1 Doppler Ultrasound

It is assumed that the reader is conversant with basic ultrasound theory and the concept of near and far fields. An introduction is given in Chapter 7 of “*Medical Physics and Biomedical Engineering*” by Brown *et al*[12].

#### 2.1.1 The Doppler Effect

The change in apparent frequency of a sound source as a result of relative movement of the source and observer was first described by Christian Doppler in 1842; a common example is the pitch change of a train whistle as it passes a stationary observer. However the effect is also observed if sound is reflected from a moving target and it is this property that is used to measure the velocity of an object with Doppler ultrasound.

The derivation of the Doppler equation is not presented here, but can be seen in section 19.7.1 of Brown *et al*[12]. The Doppler equation for a stationary transmitter and receiver, where the ultrasound beam is reflected from a moving target is given by

$$f_D = \frac{2vf_c}{c} \cos \theta \quad (2.1)$$

where  $f_D$  is the Doppler frequency,  $v$  is the velocity of the moving object,  $c$  is the speed of sound in the medium,  $\theta$  is the angle between the ultrasound beam and the direction of motion and  $f_c$  is the carrier, or transmitted frequency.

As previously discussed in section 1.3, the velocities we expect to see in this investigation are of the order of  $1.5\text{ms}^{-1}$ . If this is combined with a trans-

mitter frequency of 8MHz and it is assumed that water is the test medium ( $c = 1500ms^{-1}$ ) with no angle between the ultrasound beam and the velocity vector (i.e  $\theta = 0$ ), it is expected that the Doppler frequency obtained would be 16kHz. This is at the upper end of the normal human audible frequency range.

### 2.1.2 Doppler Systems: Overview

Doppler Ultrasound devices are now commonly used in a clinical situation for the monitoring of the cardiovascular system. For example, a simple continuous wave (CW) Doppler unit can be used to detect the movement of blood in vessels to aid diagnosis of arterial disease.

The majority of Doppler devices can be classified into one or more of the following categories:

1. Velocity detecting systems
2. Duplex systems
3. Profile detecting systems
4. Velocity imaging systems

Velocity detecting units are the simplest of the Doppler systems, and produce an output signal related to the velocity of an object (or objects) in a single sample volume. These type of systems are often hand-held, but depending on the system, can produce a non-directional audio output, or directional signals from a predetermined depth in tissue. The other systems combine pulse-echo imaging with a velocity detecting system in varying amounts to provide the user with images of flow characteristics.

Since a velocity detecting type of system is not combined with an imaging system, the angle of insonation<sup>1</sup>,  $\theta$ , between the ultrasound beam and the direction of blood flow is generally not known and their outputs cannot generally be calibrated in absolute terms. They can be used to detect the presence or absence of flow in a region and they may also be used to make velocity measurements where the angle  $\theta$  can reliably be estimated to be small.

---

<sup>1</sup>illumination by ultrasound

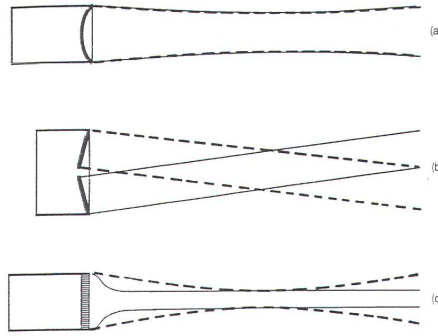


Figure 2.1: Transmission field (dashed lines) and reception zones (solid lines) of (a) single element, (b) dual element and (c) multi-element transducers

### 2.1.3 Continuous Wave Doppler Systems

All Doppler systems can also be put into one of two further categories: Continuous Wave (CW) or Pulsed Wave (PW). CW systems both transmit and receive ultrasound continuously, and therefore have no real range resolution. Also, since the transmission is continuous, separate transmitter and receiver crystals are required, although they are often housed in the same probe, adjacent to each other.

### 2.1.4 Ultrasound Transducers, Fields and Beams

As with ultrasonic imaging, the performance of the transducer is important; in Doppler applications a poor transducer can result in spurious flow signals, or noise in the signal due to low sensitivity.

The Doppler detection zone is the region in front of the transducer in which movement may be detected. The shape of the detection zone is determined by a combination of the shape of the zone into which the ultrasound is transmitted, and the reception zone (See figure 2.1). With a dual element transducer, the shapes of the transmission zone and reception zone are often similar, but are orientated to converge in front of the transducer; the primary detection zone is then the region of overlap.

A dual element transducer, as used in many CW Doppler systems is shown in figure 2.2. The two elements are fixed so that their faces are at an angle to each other. One element would act as the transmitter, and the other as the receiver, with their respective fields overlapping in a region in front of the transducer.

When the elements are placed side-by-side, they are usually D-shaped (known as a split-D) or rectangular.

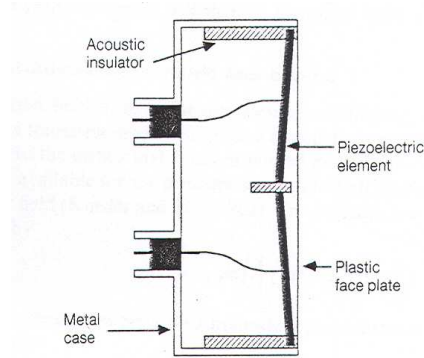


Figure 2.2: Schematic of a dual element transducer for the generation and detection of CW ultrasound

## 2.2 Huntleigh MD2 Hand-held Doppler Ultrasound Machine

The Doppler Ultrasound machine used throughout his project was a Huntleigh Healthcare Multi-Dopplex II (MD2) hand-held unit. The unit has an integral loudspeaker and headphone output.



Figure 2.3: Huntleigh MD2 Doppler Ultrasound machine

The probe supplied with the unit was the VP8, 8MHz version. This type of probe is usually used for the examination of peripheral vessels and has a region of peak sensitivity at around 20mm from its tip[13]

This unit was available in the department for us to use as it was not in clinical use.

Since there was no data available to us, it was necessary to determine the field and its Doppler frequency response. These investigations are described later in this report in sections 3.1 and 3.3 respectively.

### 2.3 Membrane Hydrophone

A membrane hydrophone is a laminated structure made up of two layers of very thin (typically  $15\mu\text{m}$ ) PVDF, a type of polycarbonate, on to which gold electrodes have been deposited, such that, only a small central area is piezoelectrically active. The active element is sandwiched between two earthed planes. This gives a sensing device that is acoustically transparent and can be used to plot the pressure distribution of ultrasonic fields.

PVDF hydrophones have an inherently wide bandwidth, typically over the frequency range 200kHz to 40MHz.

The hydrophone is connected through a powered pre-amplifier to an oscilloscope to allow the signal to be viewed.



Figure 2.4: Membrane Hydrophone

### 2.4 Laptop Computer and Sound Card Input

The Laptop computer used for data acquisition throughout this investigation was a Toshiba Satellite lap-top with an internal, integrated Realtek AC97 Audio device, running Microsoft Windows XP Home edition.

The Doppler machine was connected to the computer line-in socket by means of a stereo jack lead.

The sounds from the Doppler device were recorded using MS Sound recorder in PCM format with a sampling rate of 48.0kHz in 16-bit stereo.

## 2.5 String Phantom for Doppler Quality Assurance

The phantom used during this investigation to calibrate the Doppler machine was a Doppler Ultrasound Quality Assurance (QA) Mark 4 Doppler String Phantom by JJ&A Instruments. It is an accurate device for testing Doppler machines offering a wide range of constant string speeds (from  $10\text{cms}^{-1}$  to  $200\text{cms}^{-1}$ ) along with various pre-programmed test and physiological waveforms. There is also an integrated probe positioning clamp that can hold any Doppler probe at an angle between  $15^\circ$  and  $90^\circ$  to the string movement. It was noted that the phantom used in this investigation had a main pulley twice the diameter of the standard version, and as such, the string would be moving twice as fast as indicated on the control panel.

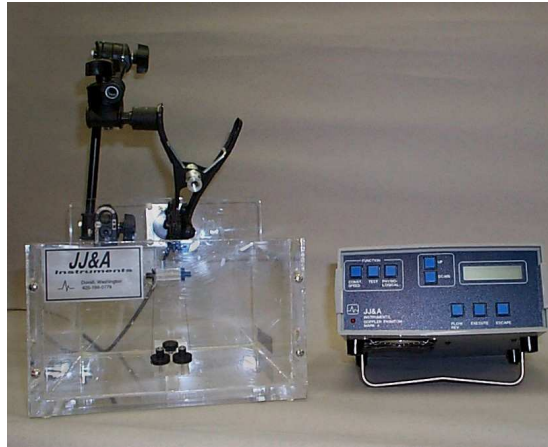


Figure 2.5: JJ&A Instruments Doppler String Phantom

## Chapter 3

# Characterisation of Doppler Machine

### 3.1 Ultrasound Beam Characterisation Using Membrane Hydrophone and Micro-Manipulator

When characterising the ultrasound beam, it is necessary to measure the beam profile at a distance representative of that which will be used at during our experiments.

#### 3.1.1 Experimental Setup

The equipment used is shown in figure 3.1. This shows a water tank with the Doppler ultrasound probe placed against a membrane at the right hand end and a gantry holding and x-y-z micro manipulator. This micro manipulator held a membrane hydrophone in the water at a known position in relation to the ultrasound probe. The ultrasound probe was placed in the clamp such that the serial number near the socket was uppermost.

The x-axis was defined to be from left to right, as viewed from the ultrasound probe, the y-axis defined to be moving away from the the probe along its axis, and the z-axis was defined to be vertical looking from the probe.

#### 3.1.2 Experimental Procedure

The active element of the hydrophone was visually lined up with the centre of the probe and the x, y and z positions, as noted from the vernier scales were recorded. At the y=0 position on the scale, the hydrophone was measured to be 2.0cm from the tip of the probe.



Figure 3.1: Experimental set-up for the beam-profiling showing the water tank with the positioning gantry over the top holding the membrane hydrophone. The Doppler probe can just be seen inserted in the Right-hand end of the tank.

It was necessary to do some preliminary calculations, these included calculating the theoretical distance  $L$  from the probe of the near-field–far-field boundary for the ultrasound probe. This was done using the following equations for a simple piston-type ultrasound transmitter

$$L = \frac{r^2}{\lambda} \quad (3.1)$$

$$\lambda = \frac{c}{f} \quad (3.2)$$

where  $r$  is the radius of the transmitter crystal,  $\lambda$  is the wavelength of the transmitted beam and  $c$  &  $f$  are the speed of sound in the medium and the frequency of the wave respectively.

It was decided initially to investigate the field at the closest end of the far field to get an initial idea of the amplitude of the ultrasound field.

The near field—far field boundary was calculated, using equation 3.1 to be at around 2.1cm from the probe. This used the following assumptions:

- The external diameter of the probe tip was measured to be 8mm.
- The transmitter/reciever crystal is assumed to be a ‘split-D’ arrangement

- The transmitter portion of the crystal is assumed to be circular for ease of calculation, therefore the radius of the transmitter crystal was taken to be 2mm.
- The transmitted frequency of the probe is 8MHz
- The speed of sound in water was approximated to be  $1500\text{ms}^{-1}$ .

This distance to the near-field/far-field boundary is a similar magnitude to the region of maximum sensitivity described in section 2.2.

Several results were collected near the probe in the far-field, to gain an appreciation for the magnitude of the field. The hydrophone was then moved out to around 11cm since this is the distance at which the ultrasound probe will be expected to work later in the project.

Three planes, perpendicular to the ultrasound beam, were recorded at 10cm, 11cm and 12cm from the probe so that a beam-profile can be calculated at this region of interest. The hydrophone was moved along the x and z axes until a maximum was found to appear on the oscilloscope. This point was taken to be the beam centre. From this point, the amplitude of the wave at each point, as displayed on the oscilloscope (in mV) was recorded.

### 3.1.3 Results

During the investigation of the field close to the probe, it was found that the maximum peak-to-peak voltage displayed on the oscilloscope was around 25 to 30mV. The field at around 11cm from the probe had peak-to-peak voltages of around 15mV. The frequency, as calculated from the oscilloscope display was 8MHz as expected.

The zero point (i.e. the point from which all measurements are related) was measured to be 15.17cm, 0.0cm, 2.19cm on the x-, y- and z-scales respectively. The beam profile for the hydrophone placed 10cm from the Doppler probe is shown in figure 3.2. Similar plots are shown in figures 3.3 and 3.4 for 11cm and 12cm distance from the probe. Note that the units of signal amplitude shown in the key are mV.

Figures 3.2, 3.3 and 3.4 show the centre of the ultrasound beam to be around 1.0–1.3cm to the left of the centre point. Using trigonometry, this equated to an off-axis skew of around  $6.2^\circ$ .

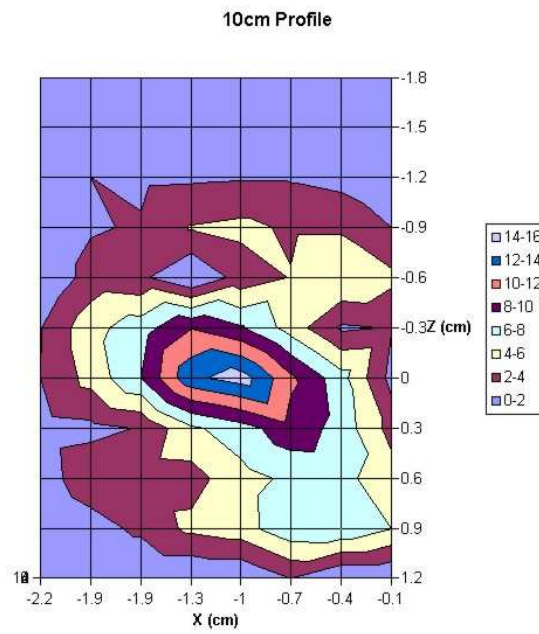


Figure 3.2: Ultrasound beam profile at 10cm from Doppler probe

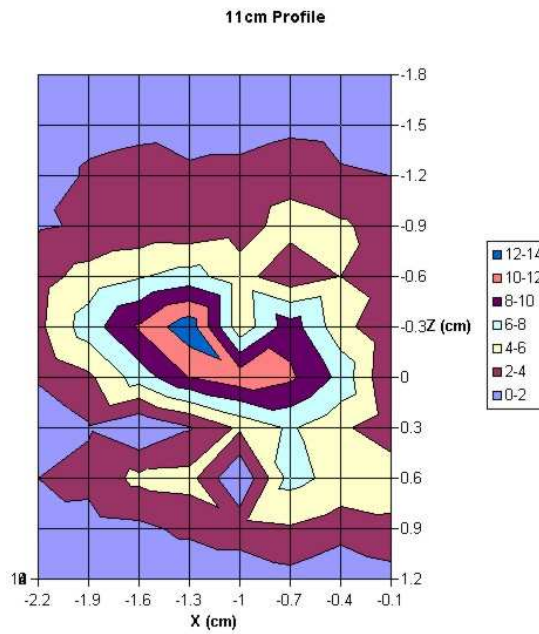


Figure 3.3: Ultrasound beam profile at 11cm from Doppler probe

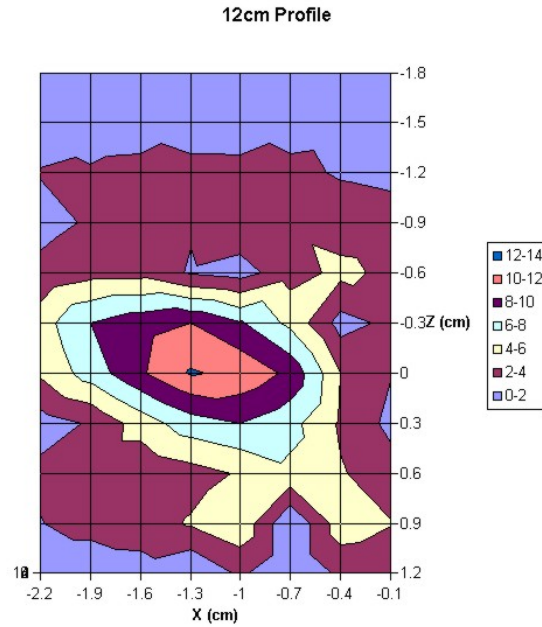


Figure 3.4: Ultrasound beam profile at 12cm from Doppler probe

The point-by-point differences between each plane were taken, and the mean of the differences was calculated to be  $-0.10\text{mV}$  for the difference between the 11cm profile and the 10cm profile, with a standard deviation (SD) of  $1.90\text{mV}$ . The mean of the differences between the 12cm and 11cm profiles was  $-0.03\text{mV}$  with a SD of  $1.83$ . For each point, the number of SDs of the difference from the mean of the differences was calculated and is plotted in figures 3.5 and 3.6. It can be seen from these figures that there is a few points around the centre where there is a significant difference from one plane to the next.

## 3.2 Determination of the Audio Card Response

To ensure that the computer was capable of capturing audio data at a sufficiently high rate, it is necessary to test the audio input and recording systems, by connecting the input of the computer to a signal generator.

### 3.2.1 Experimental Methods

The output of a signal generator was connected to the line input of the laptop computer sound card. A few seconds of the signal was recorded as a Microsoft

Plot showing point-by-point, the number of SDs from the Mean of the differences between 11cm and 10cm profile

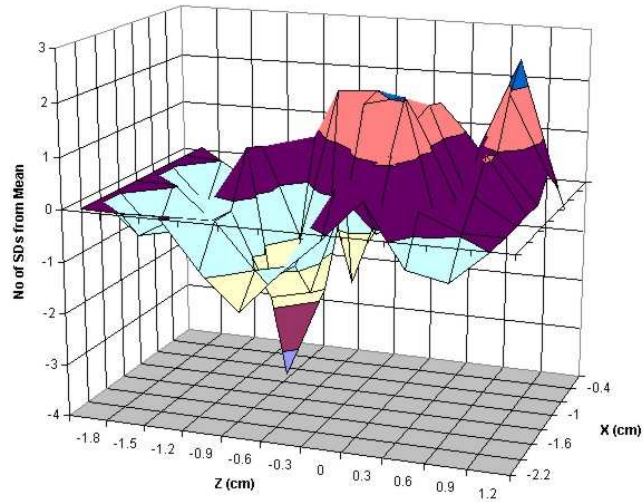


Figure 3.5: Plot showing the number of SDs of each point from the mean for the 11–10 differences

Plot showing point-by-point, the number of SDs from the Mean of the differences between 11cm and 12cm profile

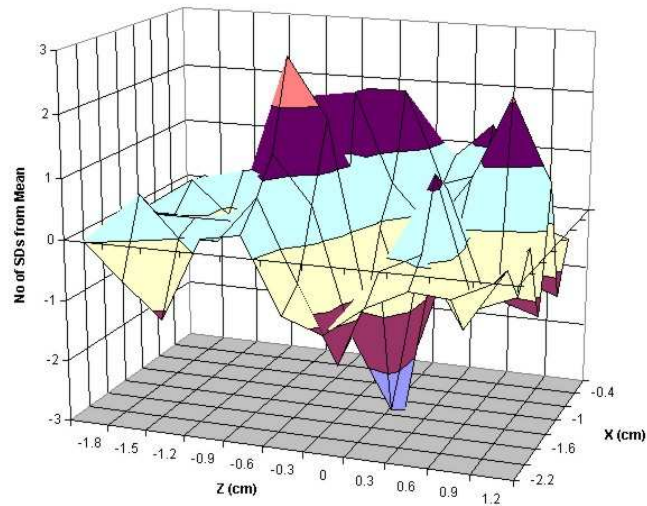


Figure 3.6: Plot showing the number of SDs of each point from the mean for the 12–11 differences

Windows .WAV file using the PCM format with a sampling rate of 48.0kHz in 16-bit stereo.

Several frequencies (5–30kHz) were recorded separately and analysed. This range was chosen since it was assumed that the sound card would easily be able to record the lower end of the audible frequency spectrum, but the response would begin to roll-off or alias at higher frequencies. It was expected from sampling theory that aliasing begins to occur at around half the sampling frequency. As shown in section 2.1, the upper limit of the expected Doppler frequency is 16kHz, so it is expected that with a sampling rate of 48kHz, this will easily be recorded.

### 3.2.2 Signal Processing Methods

Once a sample was recorded, some signal processing was necessary using MATLAB to extract information from the signal. Methods employed included time-windowing and the Fast Fourier Transform (FFT) to get a frequency spectrum. The MATLAB program used for this part is shown in Appendix B.1

The signal was read into MATLAB using the syntax

```
[sig,fs] = wavread('D:\Sound\signal generator\20k');
```

The `wavread` function is a standard MATLAB function to read in a windows .WAV file specified by the string argument and returns the sampled data in `sig` and the sampling rate (`fs`) in Hz. The sampled data `sig` is arranged in two columns, the first representing the left audio channel, and the second representing the right audio channel.

The raw signal was plotted to ensure that it was not clipped as this would introduce artifacts into the frequency spectrum. The range of the sampled data should be between  $-1$  and  $+1$ .

To get a frequency spectrum, a FFT was performed on one channel of the data. The frequency relating to each individual position in the FFT vector was calculated using the following equation

$$f = \frac{n}{N} f_s \quad (3.3)$$

where  $n$  is the position in the FFT vector,  $N$  is the number of samples in the FFT (For this part, this was set to the entire length of `sig`) and  $f_s$  is the sampling frequency, read from the .WAV file itself. For example, if the signal was

50,000 samples long, sampled at 48,000Hz, then position 2500 would represent a frequency of 2,400Hz.

According to sampling theory it is expected that all frequencies up to the Nyquist frequency ( $f_s/2$ ) should be fully reproducible after sampling. Since a sampling rate of 48.0kHz is being used, it is expected that frequencies up to 24kHz should be present in the sampled data.

The frequency spectrum was plotted and the position of the peak noted and compared to the input frequency.

### 3.2.3 Results

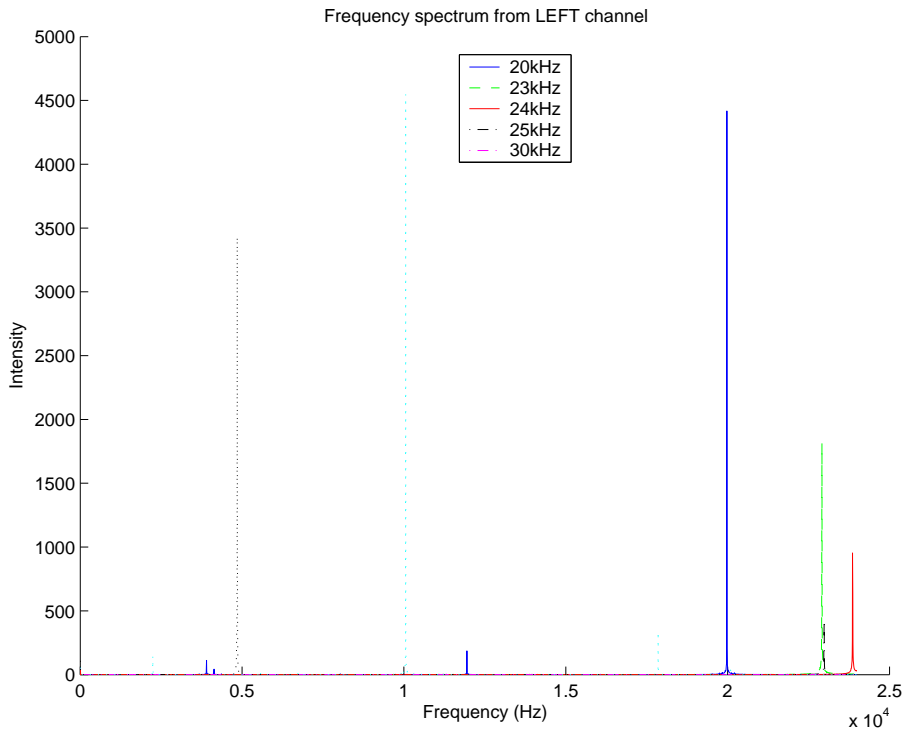


Figure 3.7: Plot showing the response of the laptop computer sound card by FFT

Figure 3.7 shows the results of the FFT of various frequency input signals. It can be seen that the first three lines (at 5kHz, 10kHz and 20kHz) are all of a similar magnitude. The peaks at 23kHz and 24kHz are lower in amplitude. This may be because the input to the sound-card may have a low pass filter with a cut-off frequency at around 22kHz (the accepted upper frequency audible to

humans). It can be seen that the 25kHz peak is of a reduced amplitude, and is aliased round to the same position as the 23kHz. The 30kHz line is flat. This may be either because of an input filter, or aliasing artifacts, or a combination of both.

### 3.3 Determination of the Doppler Response using a String Phantom

The aim of this investigation is to study the relationship between the velocity of an object and the Doppler frequency output of the unit, and to compare this with the predictions from Doppler theory, presented previously in section 2.1.1

#### 3.3.1 Experimental Methods

The equipment was set up in accordance with the instruction on the JJ&A Instruments web-site[14]. The angle between the axis of the beam and the string was noted to be  $30^\circ \pm 3^\circ$ .

For each selected string speed in the range (noting that the string is moving twice as fast as displayed on the control panel), approximately 10 seconds of the Doppler signal was recorded into the computer. These data were then processed in an exactly analogous way to those from the computer input tests described above in section 3.2. The obtained Doppler frequency,  $f_D$  was recorded and compared to the expected Doppler frequency,  $f_{D_e}$ . The correlation coefficient was calculated according to the statistical methods described below in section 3.3.2.

#### 3.3.2 Statistical Methods

Since a relationship between the Doppler frequency and the string velocity was expected, some statistical analysis was required of the results obtained. These analyses included calculation of the correlation coefficient and regression analysis. The regression analysis was required to enable the speed of the object to be back-calculated from the Doppler frequency.

##### Correlation Coefficient

The correlation coefficient is an indication of the degree of linear association between two sets of data. This may be seen visually by plotting the data on a scatter-graph.

The calculation of the correlation coefficient,  $r$ , is as follows[15], with  $x$  representing the independent variable and  $y$  the dependent variable (in this case, speed and Doppler frequency respectively).

$$r = \frac{\sum(x - \bar{x})(y - \bar{y})}{\sqrt{[\sum(x - \bar{x})^2 \sum(y - \bar{y})^2]}} \quad (3.4)$$

This can be shown[15] to equal

$$r = \frac{\sum xy - n\bar{x}\bar{y}}{(n - 1)\text{SD}(x)\text{SD}(y)} \quad (3.5)$$

where  $n$  is the number of points and  $\text{SD}(x)$  is the standard deviation of  $x$ .

To test whether the association may have arisen by chance, use the  $t$ -test in the following form[15]:

$$t = r\sqrt{\frac{n - 2}{1 - r^2}} \quad (3.6)$$

This number can be looked up for  $n - 2$  degrees of freedom in any standard statistics tables.

### Regression Analysis

Correlation describes the strength of a relationship between one variable and another. However, where the two variables are related, the dependent variable will change by a value proportional to that by which the independent variable has changed; correlation is assured.

The regression equation representing the value of the proportional variation of  $y$  in relation to  $x$  can be used to construct a regression line on a scatter plot. In the simplest case, this is assumed to be a straight line. The equation of this line can be expressed in the normal way:  $y = a + bx$ , where  $a$  is the intercept of the line on the  $y$ -axis and  $b$  is the slope of the line. These parameters must be estimated from the data as follows:

$$b = \frac{\sum(x - \bar{x})(y - \bar{y})}{\sum(x - \bar{x})^2} \quad (3.7)$$

$$a = \bar{y} - b\bar{x} \quad (3.8)$$

In a similar manner to above, it can be shown that:

$$b = \frac{\sum xy - n\bar{x}\bar{y}}{(n - 1)\text{SD}(x)^2} \quad (3.9)$$

This is a more useful method since all the components of this have already been calculated during the determination of the correlation coefficient.

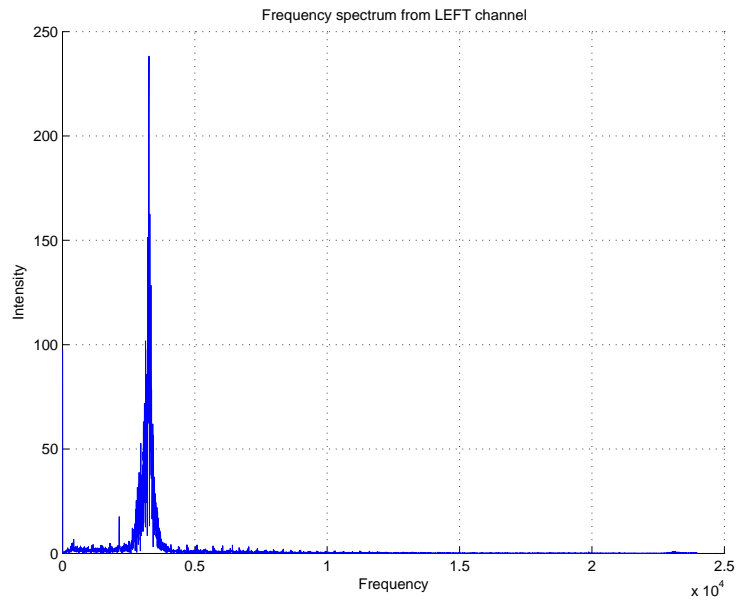


Figure 3.8: Plot showing the Doppler frequency,  $f_D$ , distribution for a string speed of 20cm/s

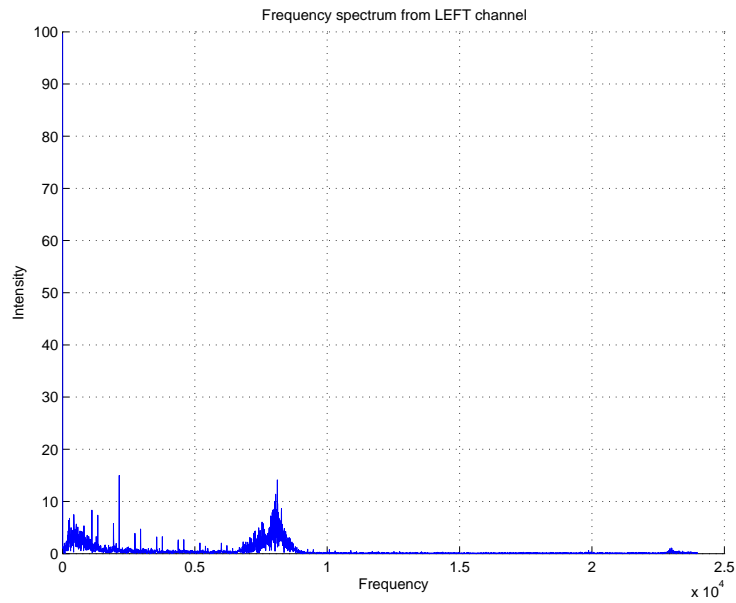


Figure 3.9: Plot showing the Doppler frequency distribution for a string speed of 50cm/s

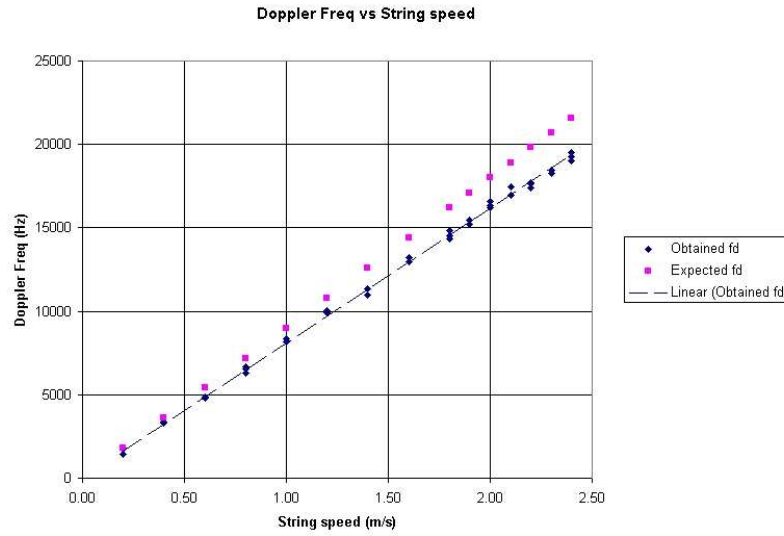


Figure 3.10: Doppler frequency as a function of string speed

### 3.3.3 Results

Figures 3.8 and 3.9 show the Doppler frequency distribution as recorded from the Doppler machine measuring the string phantom at 20cm/s and 50cm/s respectively. Note the different scales of the vertical axis. It can be seen that there is a finite width to the main peak, and figure 3.9 shows the presence of what could be  $1/f$  noise in the signal.

Figure 3.10 shows the Doppler frequency response for different string speeds. The diamonds show the frequency obtained from the Doppler unit, while the squares show the expected values for the associated string speed.

From the statistical analysis described above with the data entered into Microsoft Excel, the correlation coefficient, calculated using equation 3.5 was found to be 0.9994, while the  $b$  and  $a$  coefficients, calculated using equations 3.9 and 3.8 were calculated to be 8000.7 and 150.2 respectively. The dashed line shown in figure 3.10 was put in place by using the MS Excel “Add Trendline” feature. The coefficients Excel calculated for this line agreed with those manually calculated.

Since these coefficients were to be used in the calculation of a speed from the Doppler frequency, it was decided that this line should be forced through the origin of the graph; when there was no Doppler signal, the speed would also

be calculated to be zero. Since the automatic trendline coefficients agreed with those manually calculated, it was decided that the new coefficients could be taken from the trendline if it was forced through zero. The intercept of this new line would be zero, and the slope was seen to be 8084.4. Using the constants from equation 2.1 and the assumption that the speed of sound in water is the same for that of soft tissue ( $1540\text{ms}^{-1}$ ) the slope of the line was expected to be 8997.7.

## Chapter 4

# Using a Heart Valve Accelerated Rate Wear Tester to Measure the MHV Closure Event

### 4.1 The Shelhigh Accelerated Rate Wear Tester

#### 4.1.1 Description of Accelerated Wear Systems

Accelerated fatigue tests are required to characterise the expected life of a cardiac valve prosthesis. They assess the mechanical durability of the valve and provide information about the wear and failure modes of the devices in a reasonably short time.

There are two types of heart valve accelerated fatigue systems available in the department:

1. The system developed by The University of Sheffield, which is capable of testing six valves simultaneously.
2. The Shelhigh system, a commercially available system, also with a six valve capacity.

With the Sheffield system, a valve is mounted on top of a piston that moves vertically in a cylindrical chamber. A sine-wave excitation drives a vibrator plate at around 1200 cycles per minute. For this investigation, the Doppler probe would have to be mounted on the top of the main cylinder block. Due to the vertical motion of the valve in this system, complex signal processing and

gating of recorded data would be needed. Its fixed rate of running is also a disadvantage.

In the Shelhigh accelerated rate fatigue tester (figure 4.1) each of the six valves is mounted in an acrylic chamber that forms part of a loop. Fluid is accelerated by bellows attached to a reciprocating plate that in turn is connected to a cam on a DC motor. Above the bellows at one end of the loop there is an adjustable plug, used to adjust the pressure drop across the valve under test. For the duration of these tests, this plug remained in the fully opened position. The rate can be adjust continuously from 0 to in excess of 2000 beats per minute (bpm), although when set to lower than about 70bpm, the system does not run evenly. For this investigation, the Doppler probe was mounted on one of the end panels of one of the loops as shown in figure 4.2. The others were removed for the duration of this test.



Figure 4.1: The Shelhigh Accelerated Rate Fatigue tester showing the set-up used for this project

#### 4.1.2 Modifications to the System Required for this Project

It was decided that the Shelhigh system was the most suitable for our investigation since the valve mounting and Doppler probe would not move in relation to one another during the tests.

The only modification required was a window drilling in the end nearest the valve mount so that the Doppler probe can be mounted in a collar and held in position against a thin rubber membrane. This enabled repeatable positioning of the doppler probe.



Figure 4.2: The Doppler probe held in place at one end of the Shelhigh Wear tester

There was no method of mounting a MHV in the Shelhigh fatigue system available to us, so a system had to be devised to hold the valve in position. Several plastic mounting rings for the Sheffield system were available which clamp the valve suture ring between two pieces of acrylic, which were then screwed together. Since these mounting rings were slightly larger in diameter than the internal width of the fatigue tester, a small amount of plastic was filed off so that a snug fit could be obtained and the mounting rings held in place in the tester by friction.

Although the beam was seen to be off-axis from the Doppler probe body by around  $6^\circ$  (see section 3.1.3) this is probably due to the transmitter crystal being mounted at an angle, as discussed in section 2.1.4 and shown in figure 2.2. It was therefore decided to mount the ultrasound probe facing along the major axis of the wear tester segment.

## 4.2 Using a Spring-Loaded Translation Valve

### 4.2.1 Experimental Methods

It was decided that initially a simple, spring-loaded valve, similar to that shown in figure 4.3 would be used in the adapted wear-tester section since this valve opens by translation alone. i.e. it moves along the line of the guide and spring, which is mounted parallel to the ultrasound beam.

Once the valve was installed, the chamber filled with tap water and all major



Figure 4.3: A simple spring-loaded valve

air-bubbles removed from the chamber, the motor was turned on and the motion of the valve was observed visually. Initially the rate was set to 70bpm, but it was noted that the valve did not open at this rate. The rate was increased slowly, and the valve was observed to open once the rate reached 120bpm. With the ultrasound probe in place and connected to the computer, samples were recorded at various rates so that a comparison could be made of the valve closing velocities at a variety of rates. It was necessary to trigger the recording using a combination of observing the valve motion and starting the recording when the valve was resting on the stop as there was no method of automatically triggering the recording available to us in the timescales involved.

### 4.2.2 Signal Processing Methods

The program used to analyse these recordings is shown in appendix B.2 and uses the MATLAB `specgram` function available from the signal processing toolbox. The help file for this function is shown in appendix C. The `specgram` function returns the time-dependent Fourier transform for a sequence, using a sliding window. It requires as its arguments the signal, a window length, the sampling rate of the signal ( $f_s$ ), a window type and a window overlap.

A window length of 512 points was chosen as it was felt that this offered the best compromise between time resolution and frequency resolution. 512 points with a sampling rate of 48kHz provides a window length of  $\frac{512}{48000} = 0.0106s = 10.6ms$ , but only 512 different frequency steps over the range 0–48,000Hz, covering nearly 100Hz/step. A window overlap of  $0.9 \times$  the window length was chosen.

The signal is read into MATLAB and split into left and right channels as before. The window length and overlap are defined and the `specgram` function is called using the syntax

```
[s_p1,f,t]=specgram(s_21,win_len,fs,hamming(win_len),ov_lp);
```

This returns an array with the time/frequency history, `s_p1`, along with a vectors containing the frequency and time elements, `f` and `t` respectively. The t-f history is plotted as an image, using the syntax `pcolor(t,f,abs(s_p1))`. The absolute value of `s_p1` is plotted as it is returned from the `specgram` function as a complex number, following the application of the FFT. A large DC offset is sometimes seen in the `specgram` image, so it was decided to eliminate this by zeroing the first row of data to eliminate false low-speed calculations.

The frequency with the highest intensity is picked out for each time step, after the application of a threshold, and is used in the calculation of the associated occluder speed.

### 4.2.3 Results

Since the valve seemed to move less than 1mm (measured by observation by eye) it was very difficult to get any reliable data using automatic methods of data extraction. It was therefore decided to squeeze the bellows by hand. It was expected that this would enable the valve to open more, and therefore create a stronger Doppler response. This difference can clearly be seen in the difference between figures 4.4 and 4.5 (Note the different scales on the axes and the different intensities of the peak point)

Figure 4.6 shows the speed-time history calculated from the data in figure 4.5.

### 4.2.4 Verification of Results

Since there was no data in the literature about the closing behaviour of a spring valve, it was necessary to validate the data obtained. This was attempted by using a standard digital video camera to capture the valve closing event, downloading the video to computer and looking frame-by-frame at the movement.

Validation proved to be quite difficult for the spring valve as even with the image magnified to full-screen, the valve appeared to move by only 1mm on the screen, which after scaling had been applied<sup>1</sup> equated to 0.33mm actual occluder movement. For the 140bpm sample, the closure happened over around 80ms( $\pm 40$ ms) equating to an occluder velocity of  $4.1\text{mms}^{-1} \pm 50\%$ . This high error occurred since the valve was only in motion for around 2 video frames and both frames were blurred, indicating occluder motion.

---

<sup>1</sup>Scaling for the spring valve was applied by knowledge that the nut at the end of the spring was 5.4mm in diameter and appeared as 16mm diameter on screen.

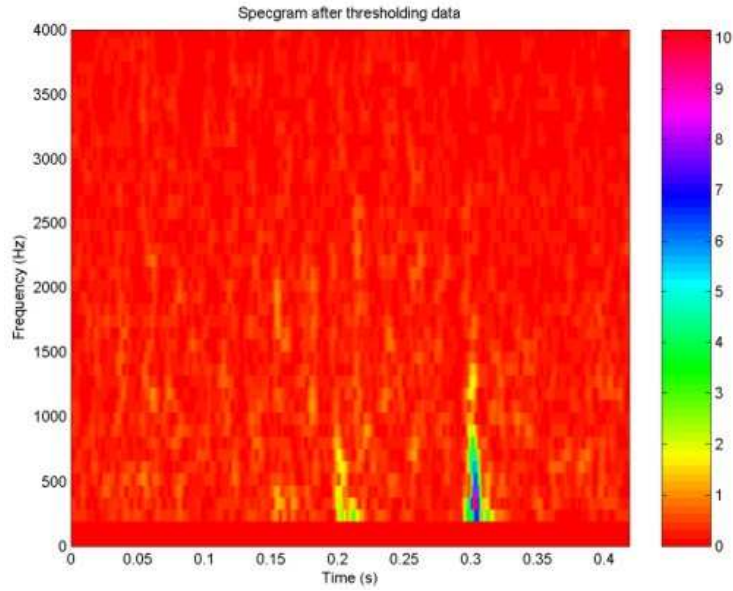


Figure 4.4: Plot showing the spectrogram of a 140rpm recoding of a spring valve

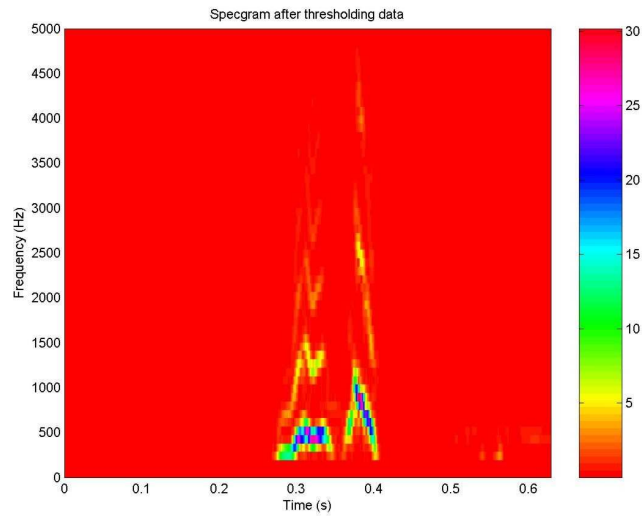


Figure 4.5: Plot showing the spectrogram of a spring valve activated by hand-squeezing of the bellows

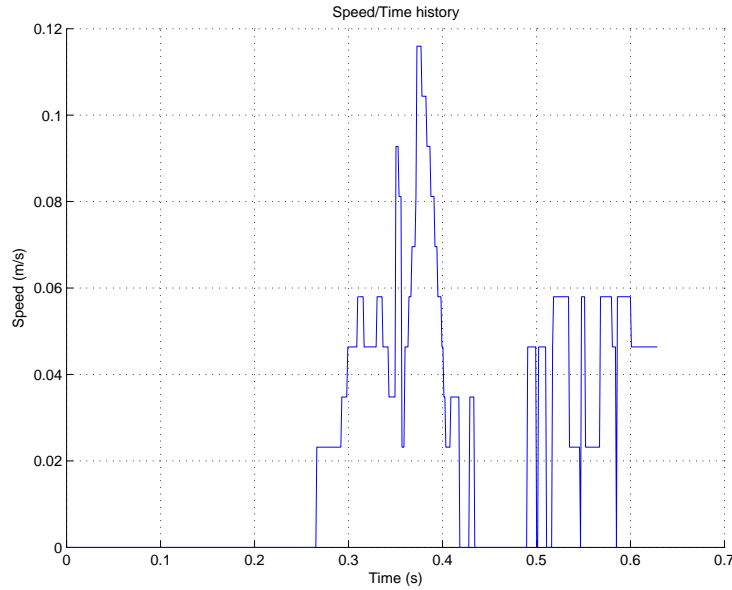


Figure 4.6: Plot showing the speed-time history of a spring valve occluder activated by hand-squeezing of the bellows

## 4.3 Using the Björk-Shiley Tilting-disc Valve

### 4.3.1 Methods

The BS valve was installed into the wear-tester and samples recorded in an exactly analogous way to the spring-valve described above in section 4.2.

After the first few samples were recorded and analysed, it became apparent that the Doppler machine was returning a wide band of frequencies. It was therefore decided that the Doppler probe should be pointed downwards in an attempt to capture data only from the tip of the occluder.

### 4.3.2 Results

#### Using Ultrasound Probe Perpendicular to Valve Plane

Figure 4.7 shows the Frequency/Time history of an opening-closing event of a BS valve with the Doppler probe parallel to the major axis of the wear-tester chamber. It can be seen that a wide band of frequencies has been captured. This is because as the valve opens and closes, the major movement is that of rotation. Therefore if the ultrasound is illuminating the whole occluder disc, there will be a complete spectrum of velocities from zero to the maximum. It

is hoped that by tilting the ultrasound probe, the tip of the occluder only can be illuminated.

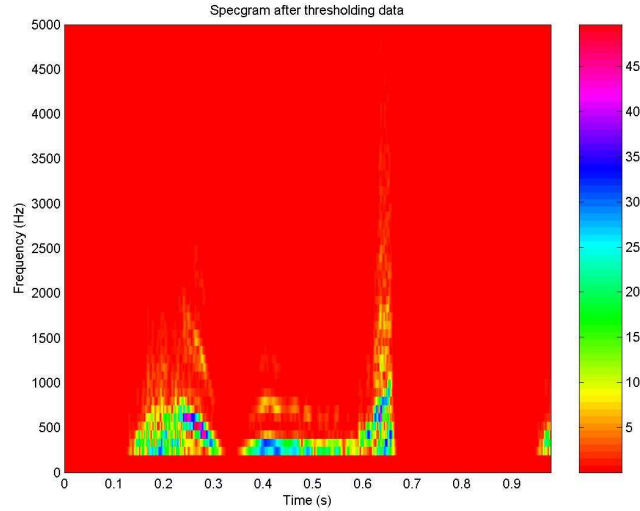


Figure 4.7: Plot showing the spectrogram of a BS valve running at 70bpm showing the opening, then the closing event

### Tilting Ultrasound Beam such that the tip is Illuminated

Figure 4.8 shows the opening-closing-opening of a BS-valve illuminated by the Doppler probe when set at an angle, such that only the tip is visible. It can clearly be seen that there is a much narrower band of frequencies present than in figure 4.7, it was therefore easier to pick out the frequency with the highest intensity for the calculation of the speed associated with that frequency. The frequency with the highest intensity was chosen (rather than the maximum frequency present) since it was noted during the experiments using the string phantom that there was a finite width to the spectrum (see figure 3.9).

Figures 4.9 to 4.12 show the speed-time history of the occluder tip for wear-tester rates of 70bpm, 90bpm, 120bpm and 140bpm respectively (note the different vertical scales). The closure event can be identified from its steep trailing edge, whereas the opening event rises, then falls steadily.

Figures 4.11 and 4.12 also show that after the main peak of the closure event, some velocities are recorded for a period of time before it returns to zero. This may be a Doppler signal received from the bounce phase of closure (described

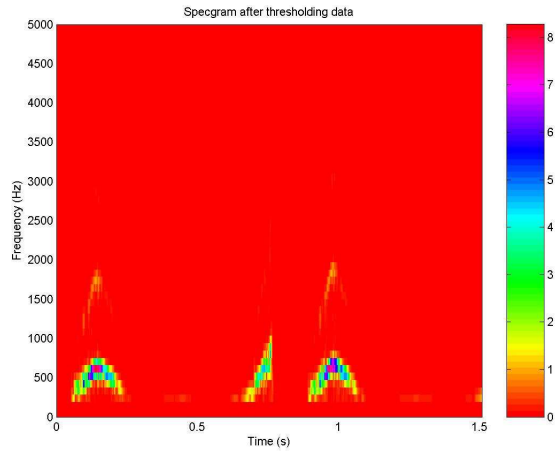


Figure 4.8: Plot showing the spectrogram of a BS valve running at 70bpm taken with the Doppler probe tilted so that it captures data from only the tip of the occluder

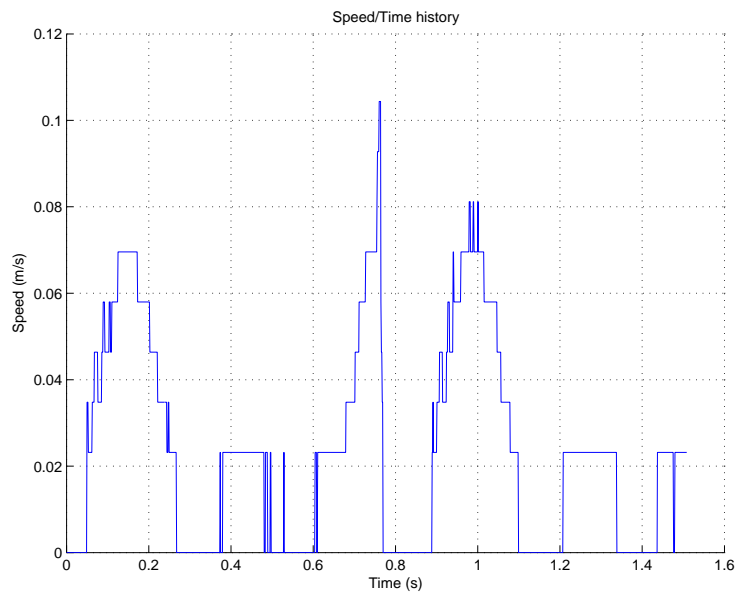


Figure 4.9: Plot showing the speed-time history of a BS valve at a rate of 70bpm

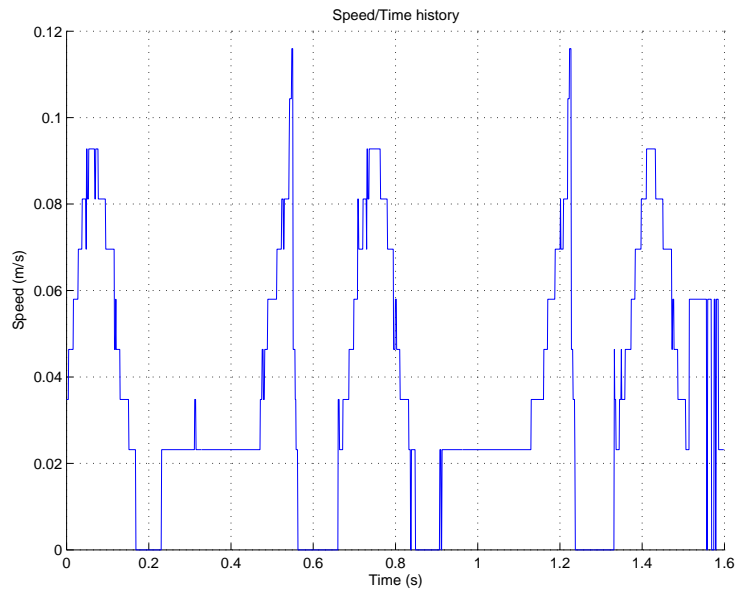


Figure 4.10: Plot showing the speed-time history of a BS valve at a rate of 90bpm

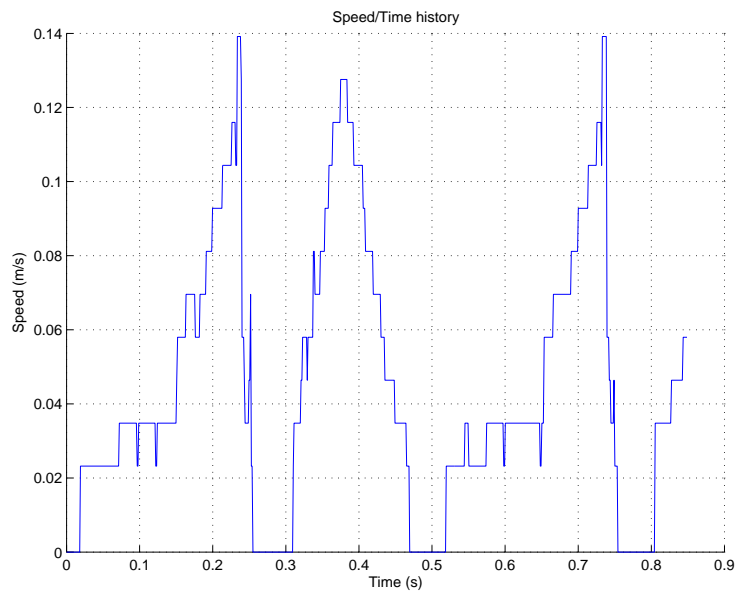


Figure 4.11: Plot showing the speed-time history of a BS valve at a rate of 120bpm

in section 1.3) or from the valve slowing down as it reaches the stop because of a *squeeze-flow* phenomenon.

Figure 4.13 shows the effect of varying the simulated heart rate on the maximum occluder velocity during the closure event.

### 4.3.3 Verification of Results

Since the stroke volume of the Shelhigh wear-test is not physiologically representative, and no pressure measurements were taken, it is unlikely that representative conditions for heart-valve closure were attained. It was noted by visual inspection of the occluder motion that the valve did not appear to open fully. This coupled with unknown pressures led us to conclude that no comparison with published data could be made. It was therefore necessary to attempt video validation with this data also. This was performed in a similar method to that for the spring valve.

During these validations, scaling was applied from the knowledge that the internal diameter of the valve orifice is 22mm and appeared on-screen as 52mm.

Verification of the results for the 29mm BS valve proved to be easier than with the spring valve as the occluder moved a significant distance and the closure event happened over the course of around three video frames. Two frames were chosen where there was definite movement and the distance the occluder moved was recorded, along with the time difference between the frames. The *average* velocity travelled in this time was calculated and found to be of a similar magnitude to that displayed in plots such as figure 4.10 (i.e. a few cm/s)

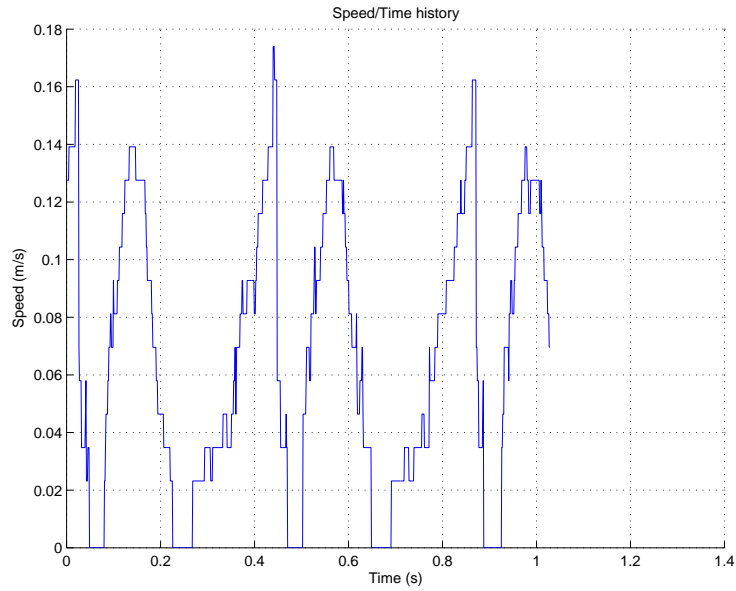


Figure 4.12: Plot showing the speed-time history of a BS valve at a rate of 140bpm

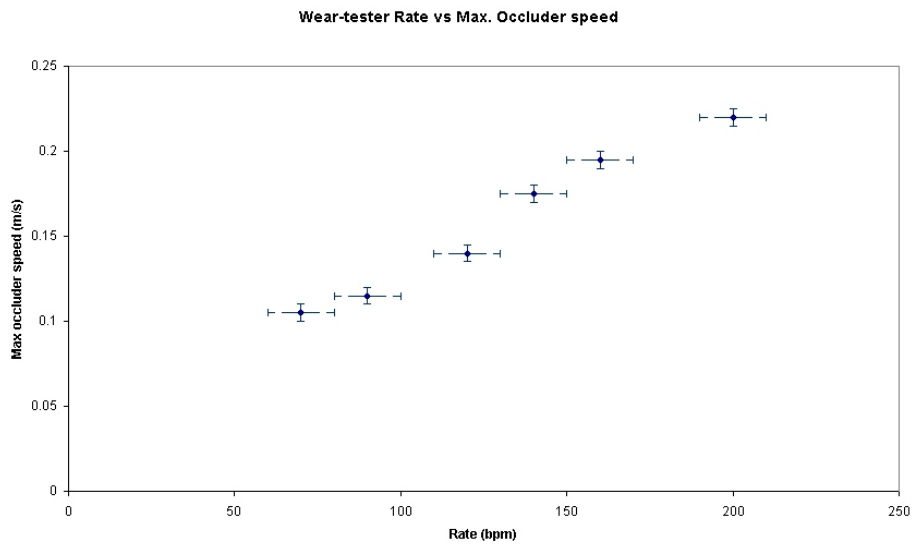


Figure 4.13: Plot showing the effect of varying the simulated heart rate on maximum occluder velocity recorded

## Chapter 5

# Conclusions and Discussion

### 5.1 US Beam from Dopplex Machine

It was shown in section 3.1.3 that the beam was tilted to the left of centre (with the serial number on the probe uppermost) by around  $6^\circ$ , however, this is most likely to be caused by the transmitting and receiving crystals in the Doppler probe being mounted at a slight angle to each other, as shown in figure 2.2. It was decided that the Doppler probe should be mounted facing parallel to the major axis of the wear tester since any Doppler signal returned from an object in this transmitted field may not be in the reception zone of the receiving crystal, particularly at the longer distances involved in the wear tester, of around 11cm.

### 5.2 Laptop Computer Audio Response

In section 3.2 it was shown that the maximum doppler frequency expected from the closure event of a BS valve was around 16kHz. From sampling theory, this would require a minimum sampling rate of 32kHz. The laptop audio card has a maximum sampling rate of 48kHz, so this would easily be able to distinguish the signal.

It was shown in section 3.2.3 that the audio system of the laptop could resolve frequencies up to 24kHz, i.e. half of the sampling rate proving that it was suitable for recording the Doppler signals.

### 5.3 Doppler Signal and Interface with PC

Section 3.3 set out the methods used to determine the Doppler response of the MD2 unit. This was achieved by connecting the headphone output socket of

the MD2 to the line-input of the laptop audio card. The results in section 3.3.3, and in particular, figure 3.10 show the calibration line used in the subsequent sections for the calculation of the velocity from a Doppler frequency. Since the slope and intercept of the original line (with a finite intercept) were the same as those produced by the MS Excel “Add Trendline” function, it was decided that the figures from MS Excel could be trusted, and the trendline was adjusted using the “properties” dialogue box so that the intercept was set to zero.

It was decided that this calibration line should be forced through the origin of the plot so that when the doppler frequency was zero, the subsequent calculation show the object to be stationary, rather than moving at some negative velocity.

The documentation for the MD2 Doppler Ultrasound machine implied that it should output a bi-directional signal. This means that forward movement should produce sound in one channel, and reverse movement, sound on the other, however under initial testing, no evidence of this was found. It was decided that this did not constitute a major problem since any sudden change in direction should manifest itself as a discontinuity in the time/frequency spectrum.

## 5.4 Using US Machine to Detect Heart Valve Motion

Using this method to measure the motion of a simple spring-loaded valve proved to be difficult since the occluder moved less than 0.5mm, however, it can be seen from section 4.3.2 that the technique can be used to measure the gross motion of a BS valve occluder. Since no automatic triggering of the recording was available to us, the signals could not be laid over one another so that a direct, graphical comparison could be made.

With the equipment available to us, and the signal processing methods described herein, we saw no conclusive proof that the bounce phase of occluder motion can be measured accurately, or even exists under the conditions attained. An appreciation of the peak occluder velocity can however be obtained from this method. Also, since no reliable triggering was utilised, no analysis of closure delay could be made.

## 5.5 Use of Doppler Techniques for Detecting MHV Failure

Doppler ultrasound is potentially a very useful tool for studying the motion of implanted MHVs. It is hoped that this technique can eventually be used as a screening tool to study the motion of heart valve leaflets *in-vivo* using transesophageal Doppler ultrasound. This would be of benefit to patients who are assessed to be at a higher risk of suffering valve failure.

## 5.6 Suggestions for Further Work

Suggestions for further work on this technique include

- Using a Pulse Duplicator (PD) to study the motion of the occluder under physiologically representative conditions using Doppler Ultrasound in a similar manner.
- Looking to improve the signal processing tools.
- Investigate some method of automatic triggering of the recording so that repetitive results can be overlaid and directly compared.

# Bibliography

- [1] R.A. DeWall, N. Qasim, and L. Carr. Evolution of mechanical heart valves. *Annals of Thoracic Surgery.*, 69:1612–21, 2000.
- [2] Vincent L. Gott, Diane E. Alejo, and Duke E. Cameron. Mechanical heart valves: 50 years of evolution. *Annals of Thoracic Surgery.*, 76:S2230–9, 2003.
- [3] Viking O. Bjork. The development of the bjork-shiley artificial heart valve. *Clinical Cardiology*, 7:3–5, 1984.
- [4] Claire Carson, Julia Richman, and Robin Creel. The physics behind artificial heart valves. <http://www.ipass.net/tonyg/HeartValvesWeb.html>, December 2000.
- [5] H. Lee, T. Tsukiya, A. Homma, Y. Taenaka, E. Tatsumi, and H. Takano. Measurement of the closing behavior of the bjork-shiley monoleaflet mechanical heart valve with an electrohydraulic total artificial heart. *Artificial Organs*, 27(8):744–8, Aug 2003.
- [6] Z.J. Wu, M.C. Shu, D.R. Scott, and N.H. Hwang. The closing behavior of medtronic hall mechanical heart valves. *ASAIO Journal*, 40(3):M702–6, Jul-Sep 1994.
- [7] G.X. Guo, T.H. Chiang, R.C. Quijano, and N.H. Hwang. The closing velocity of mechanical heart valve leaflets. *Medical Engineering and Physics.*, 16(6):458–64, Nov 1994.
- [8] K.B. Chandran and S. Aluri. Mechanical valve closing dynamics: relationship between velocity of closing, pressure transients, and cavitation initiation. *Annals of Biomedical Engineering.*, 25(6):926–38, Nov-Dec 1997.

- [9] Z.J. Wu, B.Z. Gao, and N.H. Hwang. Transient pressure at closing of a monoleaflet mechanical heart valve prosthesis: mounting compliance effect. *Journal of Heart Valve Disease.*, 4(5):553–67, Sept 1995.
- [10] K.B. Chandran, C.S. Lee, S. Aluri, K.C. Dellsperger, S. Schreck, and D.W. Wieting. Pressure distribution near the occluders and impact forces on the outlet struts of bjork-shiley convexo-concave valves during closing. *Journal of Heart Valve Disease*, 5(2):199–206, March 1996.
- [11] A.C. Eberhardt, M.A. Ward, S.J. Lewandowski, R. Inderbitzen, and D.W. Wieting. Relationships between closure delay, pressure, velocity and outlet strut forces of the bjork0shiley heart valve. *Advances in Bioengineering*, 26:547–551, 1993.
- [12] B.H. Brown, R.H. Smallwood, D.C. Barber, P.V. Lawford, and D.R. Hose. *Medical Physics and Biomedical Engineering*. IOP Publishing, 1999.
- [13] Huntleigh Healthcare Website. Doppler probes for the vascular dopplex range. [www.nesbitevans.com/AltProductFTP/UK/diagnostics/vascular/probes/index.htm](http://www.nesbitevans.com/AltProductFTP/UK/diagnostics/vascular/probes/index.htm). viewed 1st July 2004.
- [14] JJ&A Instruments Website. [www.jja-instruments.com/Using%20Mark4.htm](http://www.jja-instruments.com/Using%20Mark4.htm).
- [15] T.D.V. Swinscow and M.J. Campbell. *Statistics at Square One*. BMJ Books, tenth edition, 2002.

## Appendix A

# Project Plans

Figures A.1 and A.2 show the project plans. Figure A.1 was drawn up at the beginning of the project while figure A.2 follows some modifications. These modifications were required due to some slippage in the testing of the ultrasound machine. It took considerably longer than anticipated to profile the beam and measure the Doppler frequency response of the Ultrasound unit. There is a block of two weeks corresponding to the Easter break factored in to these time-scales where no work was carried out.

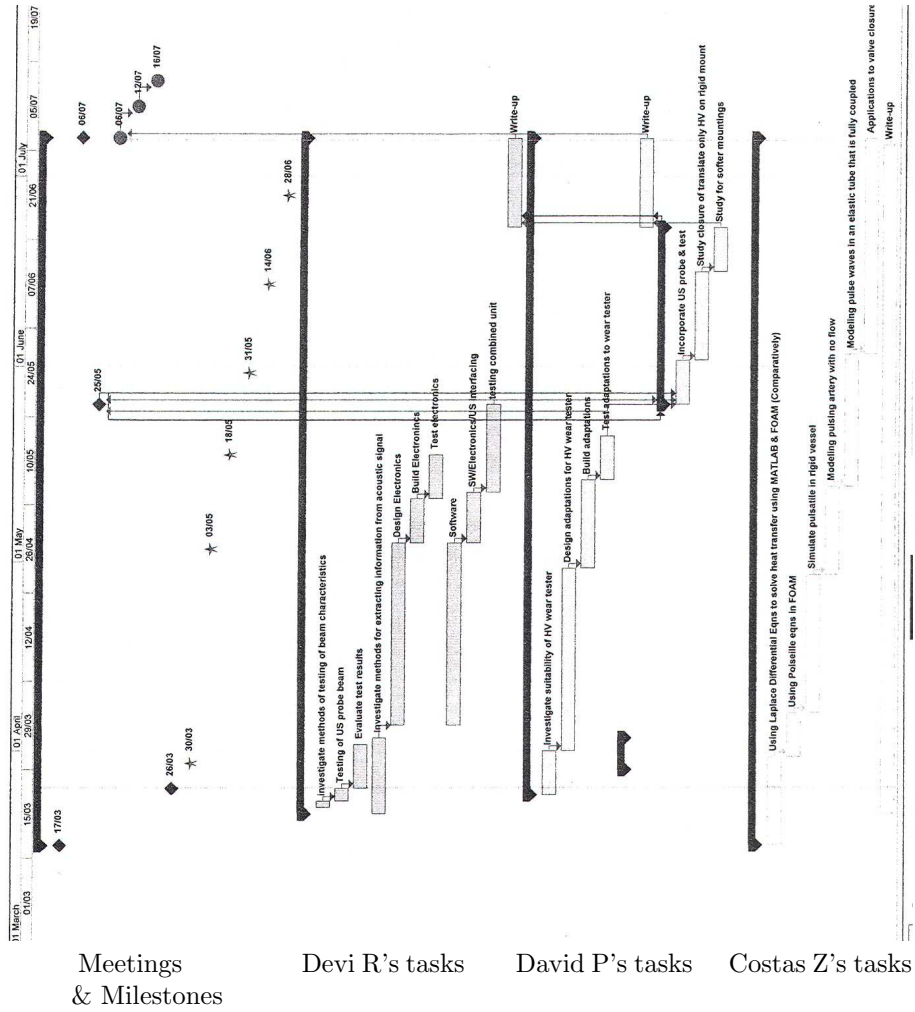


Figure A.1: Original Project plan

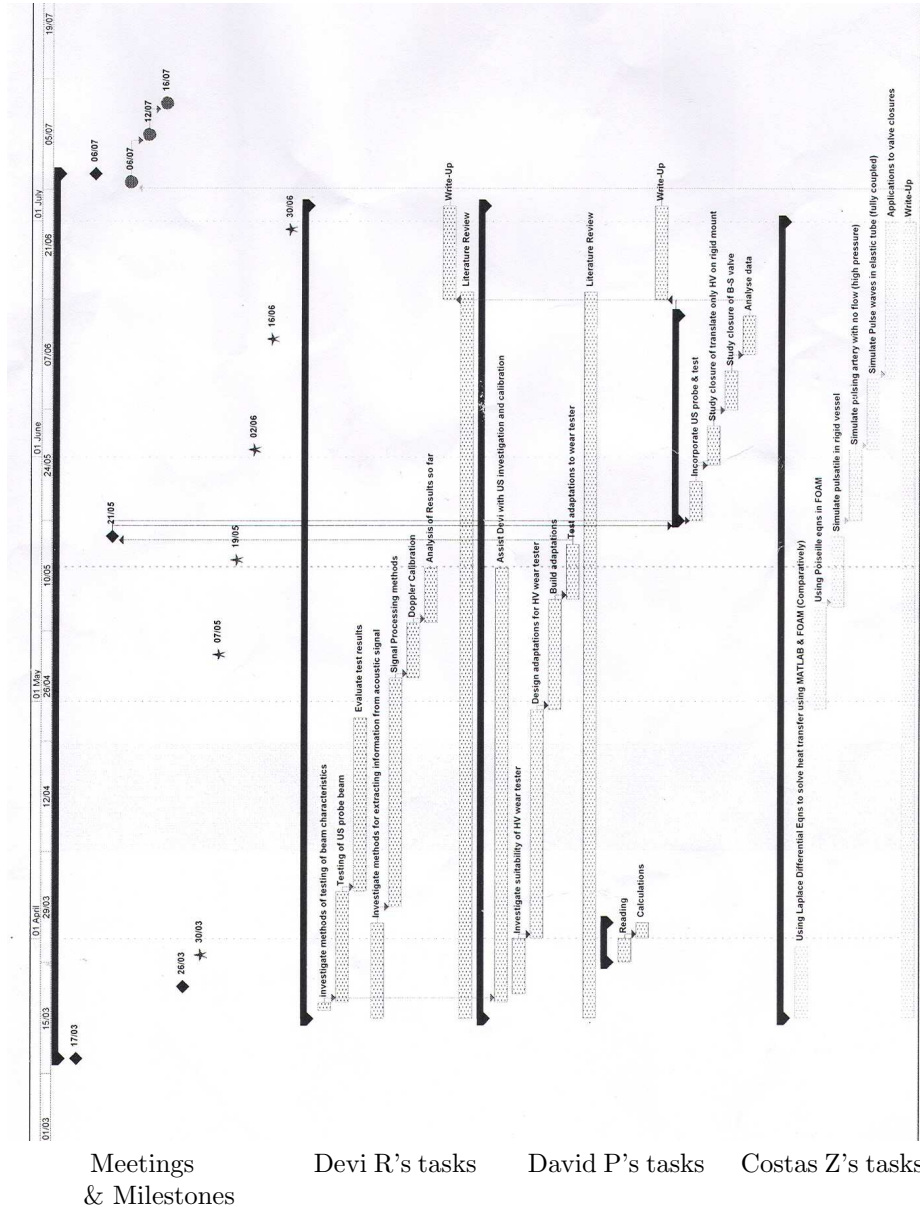


Figure A.2: Project plan after alterations to reflect changes to project progress

## Appendix B

# MATLAB Programs used

### B.1 Frequency Analysis Program

```
%Program for Frequency analysis by FFT

clear all
clc

%RAW SIGNAL
[s_2,fs]=wavread('D:\Sound\signal generator\20k');
s_21=s_2(:,1);%left channel (the 1st collumn)
figure
plot(s_21); grid on; zoom on
title('RAW SIGNAL-LEFT CHANNEL');
N=length(s_21)
s_22=s_2(:,2);%right channel (the 2nd collumn)

fftlens=512;
%RAW SIGNAL FFT
s_21orgf=fft(s_21,fftlens);%fft of the left channel
s_22orgf=fft(s_22,fftlens);%fft of the right channel
N_1=length(s_21orgf);
N_2=length(s_22orgf);
s_21orgf=s_21orgf(1:round(N_1/2));
s_22orgf=s_22orgf(1:round(N_2/2));

f=[1:round(fftlens/2)]/fftlens*fs;

figure
plot(f,abs(s_21orgf)), grid on, zoom on;
title('Frequency spectrum from LEFT channel')
```

```
xlabel('Frequency')
ylabel('Intensity')
```

## B.2 Moving Window & Speed Calculations

```
%Program to look at the freq history of a sound file
clear all
clc

col_map='hsv';

%RAW SIGNAL
[s_2,fs]=wavread('D:\Sound\BSvalve29mmtiltingUS\70rpm3');

s_21=s_2(:,1);%left channel (the 1st column)
N=length(s_21)
t=0:1/fs:(N-1)/fs;

%figure; plot(t,s_21); grid on; title('RAW SIGNAL-LEFT CHANNEL');
%zoom on;
%xlabel('Time (s)'); ylabel('Amplitude');

%APPLICATION OF THE MOVING WINDOW TO THE ABOVE RAW SIGNAL
win_len=512
ov_lp=round(0.9*win_len);
[s_p1,f,t]=specgram(s_21,win_len,fs,hamming(win_len),ov_lp);

%figure; pcolor(t,f,abs(s_p1)); shading flat; colormap(col_map);
%colorbar; zoom on;
%xlabel('Time (s)'); ylabel('Frequency (Hz)');
%title('Original Specgram')

%Sometimes, there is a massive DC offset, so just zero
%the first two rows
for i=1:2
    s_p1(i,:)=0;
end

%figure; pcolor(t,f,abs(s_p1)); shading flat; colormap(col_map);
%colorbar; zoom on;
%xlabel('Time (s)'); ylabel('Frequency (Hz)');
%title('Specgram after zeroing first two rows to get rid of DC offset')

%Calc highest peak in s_p1
max_max=max(max(abs(s_p1)))
size_sp1=size(s_p1)
```

```
%Zero any data that is less than thresh the hight of the max_max
thresh=1/100
for i=1:size_sp1(1);
    for j=1:size_sp1(2);
        if abs(s_p1(i,j)) < max_max*thresh;
            s_p1new(i,j) = 0;
        else
            s_p1new(i,j) = s_p1(i,j);
        end
    end
end

%Find the max value in each col, and its index
[s_p1max,ind]=max(abs(s_p1new));

%Plot f-t history
figure; pcolor(t,f,abs(s_p1new)); shading flat; colormap(col_map);
colorbar; zoom on;
xlabel('Time (s)'); ylabel('Frequency (Hz)');
title('Spectrogram after thresholding data')

%Find freq relating to index found earlier
s_pf=f(ind);

%Calc speed from Doppler theory
%c_sound=1540;
%fc=8000000;
%ang=0;
%vel_th=s_pf.*c_sound./((2*fc));

%Calc speed from our calibration expts
slope=8084.4;
offset=0;%forcing it thru zero;
vel_corr=(s_pf-offset)/slope;
figure; hold on; plot(t,vel_corr);grid on; zoom on;
xlabel('Time (s)'); ylabel('Speed (m/s)'); title('Speed/Time history')
```

## Appendix C

# MATLAB Specgram Function

This is a copy of the MATLAB help-file for the Specgram function that provides a time-dependent frequency analysis (spectrogram)

### C.1 Syntax

```
B = specgram(a)
B = specgram(a,nfft)
[B,f] = specgram(a,nfft,fs)
[B,f,t] = specgram(a,nfft,fs)
B = specgram(a,nfft,fs>window)
B = specgram(a,nfft,fs>window,numoverlap)
specgram(a)
B = specgram(a,f,fs>window,numoverlap)
```

### C.2 Description

`specgram` computes the windowed discrete-time Fourier transform of a signal using a sliding window. The spectrogram is the magnitude of this function.

`B = specgram(a)` calculates the windowed discrete-time Fourier transform for the signal in vector `a`. This syntax uses the default values:

- `nfft = min(256,length(a))`
- `fs = 2`
- `window` is a periodic Hann (Hanning) window of length `nfft`.
- `numoverlap = length(window)/2`

`nfft` specifies the FFT length that `specgram` uses. This value determines the frequencies at which the discrete-time Fourier transform is computed. `fs`

is a scalar that specifies the sampling frequency. `window` specifies a windowing function and the number of samples `specgram` uses in its sectioning of vector `a`. `numoverlap` is the number of samples by which the sections overlap. Any arguments that you omit from the end of the input parameter list use the default values shown above.

If `a` is real, `specgram` computes the discrete-time Fourier transform at positive frequencies only. If `n` is even, `specgram` returns `nfft/2+1` rows (including the zero and Nyquist frequency terms). If `n` is odd, `specgram` returns `nfft/2` rows. The number of columns in `B` is

$$k = \text{fix}((n - \text{numoverlap}) / (\text{length}(\text{window}) - \text{numoverlap}))$$

If `a` is complex, `specgram` computes the discrete-time Fourier transform at both positive and negative frequencies. In this case, `B` is a complex matrix with `nfft` rows. Time increases linearly across the columns of `B`, starting with sample 1 in column 1. Frequency increases linearly down the rows, starting at 0.

`B = specgram(a, nfft)` uses the specified FFT length `nfft` in its calculations.

`[B, f] = specgram(a, nfft, fs)` returns a vector `f` of frequencies at which the function computes the discrete-time Fourier transform. `fs` has no effect on the output `B`; it is a frequency scaling multiplier.

`[B, f, t] = specgram(a, nfft, fs)` returns frequency and time vectors `f` and `t` respectively. `t` is a column vector of scaled times, with length equal to the number of columns of `B`. `t(j)` is the earliest time at which the  $j$ th window intersects `a`. `t(1)` is always equal to 0.

`B = specgram(a, nfft, fs, window)` specifies a windowing function and the number of samples per section of the  $x$  vector. If you supply a scalar for `window`, `specgram` uses a Hann window of that length. The length of the window must be less than or equal to `nfft`.

`B = specgram(a, nfft, fs, window, numoverlap)` overlaps the sections of `x` by `numoverlap` samples.

You can use the empty matrix `[]` to specify the default value for any input argument. For example, `B = specgram(x, [], 10000)` is equivalent to `B = specgram(x)` but with a sampling frequency of 10,000 Hz instead of the default 2 Hz.

`specgram(...)` with no output arguments displays the scaled logarithm of the spectrogram in the current figure window using

```
imagesc(t, f, 20*log10(abs(b))), axis xy, colormap(jet)
```

The `axis xy` mode displays the low-frequency content of the first portion of the signal in the lower-left corner of the axes. `specgram` uses `fs` to label the axes according to true time and frequency.

`B = specgram(a, f, fs, window, numoverlap)` computes the spectrogram at the frequencies specified in `f`, using either the chirp  $z$ -transform (for more than 20 evenly spaced frequencies) or a polyphase decimation filter bank. `f` is a vector of frequencies in hertz; it must have at least two elements.

### C.3 Algorithm

`specgram` calculates the spectrogram for a given signal as follows:

1. It splits the signal into overlapping sections and applies the window specified by the window parameter to each section.
2. It computes the discrete-time Fourier transform of each section with a length `nfft` FFT to produce an estimate of the short-term frequency content of the signal; these transforms make up the columns of `B`. The quantity `(length(window) - numoverlap)` specifies by how many samples `specgram` shifts the window.
3. For real input, `specgram` truncates the spectrogram to the first `nfft/2 + 1` points for `nfft` even and `(nfft + 1)/2` for `nfft` odd.